



Contents lists available at ScienceDirect

Journal of King Saud University – Science

journal homepage: www.sciencedirect.com

Original article

Synthesis of 2-mercaptopropionic acid/hydrous zirconium oxide composite and its application for removal of Pb(II) from water samples: Central composite design for optimization

Nafisur Rahman^{a,*}, Mohd Nasir^a, Asma A. Alothman^b, Abdullah M. Al-Enizi^{b,*}, Mohd Ubaidullah^b, Shoyebmohamad F. Shaikh^b^a Department of Chemistry, Aligarh Muslim University, Aligarh 202002, India^b Department of Chemistry, College of Science, King Saud University, Riyadh 11451, Saudi Arabia

ARTICLE INFO

Article history:

Received 3 November 2020

Revised 28 November 2020

Accepted 6 December 2020

Available online 17 December 2020

Keywords:

2-Mercaptopropionic

Pb(II)

CCD

Adsorption

Error function

Isotherm

Kinetic

ABSTRACT

In this study, 2-mercaptopropionic acid was incorporated into hydrous zirconium oxide matrix to prepare 2-mercaptopropionic acid/ hydrous zirconium oxide (MPA/HZO) composite and applied to eliminate Pb(II) from aqueous environment. MPA/HZO was characterized by FTIR, TGA-DTA and SEM with EDX. Response surface methodology (RSM) was utilized for optimizing the independent variables affecting the uptake of Pb(II). The maximum efficiency was reached at an equilibrating time of 40 min. At the optimum conditions (pH:6.8; contact time: 40 min; adsorbent dose: 0.016 g; initial concentration: 60 mg/L), 99.37% Pb(II) was successfully eliminated. Nonlinear regression analysis was applied for the investigation of isotherm and kinetic equations. Langmuir isotherm model with $R^2 > 0.99$ was best fit model to demonstrate the adsorption of Pb(II) onto MPA/HZO. The maximum Langmuir adsorption capacity (q_m) was 128.50 mg/g. Pseudo-second order kinetic model with $R^2 > 0.999$ illustrated its best fitting to the kinetic data.

© 2020 The Author(s). Published by Elsevier B.V. on behalf of King Saud University. This is an open access article under the CC BY-NC-ND license (<http://creativecommons.org/licenses/by-nc-nd/4.0/>).

1. Introduction

The presence of non-degradable heavy metals in aquatic environment poses a serious hazard to living species. They have been discharged into superficial water from a number of industries such as electroplating, battery manufacturing, metal plating, textiles, mining, etc. (Jiang, et al., 2020). Among the heavy metals, Pb (II) is the first recognized metal pollutant in soft water due to the use of lead service pipes (Boudrahem et al., 2011). The acceptable limit of Pb (II) in drinking water according to World Health Organization (2017) is 10 µg/L. The elevated concentration of Pb (II) poses serious health problems such as nerves and renal breakdown, kidney damage, hypertension, behavioral disorders and,

convulsions (Kumar et al., 2020). Therefore, it is very important to develop effective, simple and integrated technique to decontaminate Pb (II) from contaminated water. Several techniques such as solvent extraction (Halli et al., 2020), reverse osmosis (Thaci and Gashi, 2019), coagulation (Bora and Dutta, 2019), ion exchange (Gupta et al., 2005; Lutfullah et al., 2012a, 2012b) and adsorption (Gupta et al., 2004; Rahman, et al., 2020a) have been extensively investigated to remove Pb(II) from water. Adsorption is an effective technique for the elimination of Pb(II) due to its environment friendly property, excellent performance, low cost, without releasing reaction by-product and reusable. Recently, various adsorbents such as clay mineral (Azamfire, et al., 2020) biochar (Boni, et al., 2020), biosorbent (Azmi et al., 2020) chitosan (Moja, et al., 2020) and carbon nanofibers (Nordin et al., 2020) were applied for the remediation of Pb(II) from water. Moreover, attempts have been made to prepare organic–inorganic hybrid materials to eradicate Pb (II) from aqueous medium (Rahman and Haseen, 2014; Rahman et al., 2017, 2020). In the hybrid material, various functional groups of organic substance are combined with thermally stable and robust inorganic matrix with high binding affinity towards the selected metal ions.

Response surface methodology (RSM) is widely used to study the relationship between various process variables and desired

* Corresponding authors.

E-mail addresses: nafisurrahman05@gmail.com (N. Rahman), amenizi@ksu.edu.sa (A.M. Al-Enizi).

Peer review under responsibility of King Saud University.



Production and hosting by Elsevier

<https://doi.org/10.1016/j.jksus.2020.101280>

1018-3647/© 2020 The Author(s). Published by Elsevier B.V. on behalf of King Saud University.

This is an open access article under the CC BY-NC-ND license (<http://creativecommons.org/licenses/by-nc-nd/4.0/>).

responses simultaneously. Recently, the variables of adsorption processes were optimized by RSM via Box-Behnken design (Rahman and Nasir, 2018; Rahman and Varshney, 2020; Rahman et al., 2021) or central composite design (Rahman and Nasir, 2019; Rahman and Nasir, 2020a, 2020b). In RSM, less number of experiments is required for optimization of variables as compared to conventional method of optimization. In this study, 2-mercaptopropionic acid/ hydrous zirconium oxide (MPA/HZO) composite was synthesized. Central composite design (CCD) was tried to optimize the variables of adsorption process (pH, adsorbent dose and initial concentration) for obtaining the highest removal of Pb(II). Various isotherm and kinetic models were subjected to experimental data to find out the nature of adsorption.

2. Experimental

2.1. Reagents

For the synthesis of MPA/ HZO composite, 2-mercaptopropionic acid and ammonia solution (25%) were obtained from Merck Specialties Pvt. Ltd, India. Zirconium oxychloride and lead nitrate were procured from Otto Chemie Pvt. Ltd, India. All other materials used in the experiments were analytical grade.

2.2. Instruments

Atomic absorption spectrophotometer (GBC Scientific, model 932 Plus, Australia) and pH meter (Cyberscan pH 2100) have been used to estimate the Pb(II) concentration and pH, respectively. PerkinElmer FTIR spectrophotometer (Spectrum 2) was used to obtain FTIR spectra. Simultaneous thermogravimetry–differential thermal analysis (TGA–DTA) were performed using Shimadzu thermal analyzer (DTG 60H) in nitrogen atmosphere with heating rate of 10 °C/min. SEM images with EDX spectra were obtained with JEOL scanning electron microscope (JSM-6510LV). The temperature and shaking speed was monitored in water bath shaker (Narang Scientific Works, India).

2.3. Synthesis of 2-mercaptopropionic acid/hydrous zirconium(IV) oxide (MPA/HZO) composite

The MPA/HZO was synthesized in two steps. In the first step, hydrous zirconium oxide (HZO) was prepared at room temperature by slow addition of 6% ammonium hydroxide to aqueous solution of zirconium oxychloride (0.10 mol/L) in equal proportion. In the second step, 2-mercaptopropionic acid (0.10 mol/L in ethanol) was mixed with HZO in 3:1 proportion with maintaining the pH 6 and stirred for 24 h and filtered after washing with distilled water and ethanol. The material was kept in an oven at 40 °C for drying. The schematic diagram for the preparation of MPA/HZO is given in Scheme 1.

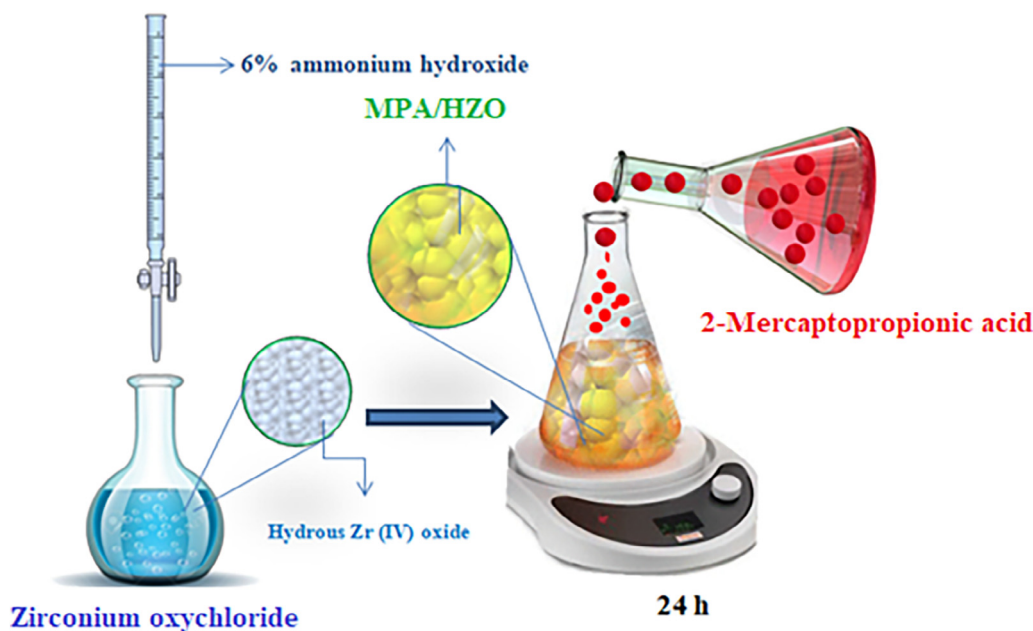
2.4. Design of experiment and statistical analysis

CCD was used to study the impact of the independent variables on the removal of Pb (II). Three process variables such as pH (X_1), adsorbent dose (X_2) and initial concentration (X_3) were examined to obtain the highest Pb (II) removal efficiency. The ranges and levels of variables used in CCD are given in Table S1 (Supplementary material). The CCD matrix was generated by Design Expert software (free trial version 12.0.0) for three factors, each factor at five levels ($-\alpha$, -1 , 0 , $+1$ and $+\alpha$) and the total number of experimental runs can be computed using Eq. (1) (Rahman and Nasir, 2018):

$$E_N = 2^n + 2n + n_c \quad (1)$$

where E_N and n are total experimental runs and number of factors, respectively. Therefore, a total 20 experimental runs are required to optimize the adsorption process. The experiments were completed according to the CCD matrix involving different combinations of independent variables and the results (Table 1) were analyzed by multi-regression analysis. The predicted responses (removal %) can be obtained from Eq.(2):

$$Y = \beta_0 + \sum_{i=1}^k \beta_i X_i + \sum_{i=1}^k \sum_{j=1}^k \beta_{ij} X_i X_j + \sum_{i=1}^k \beta_{ii} X_i^2 + \varepsilon \quad (2)$$



Scheme 1. Schematic routes for synthesis of MPA/HZO composite.

Table 1
Central composite design matrix and experimental and predicted values (response) of Pb (II) removal (%) by MPA/HZO.

Exp. Run	Space type	Coded factors			Uncoded factors			Observed response (%)	Predicted response (%)
		X ₁	X ₂	X ₃	pH	Adsorbent dose (g)	Initial concentration (mg/L)		
1	Axial	0	0	+α	6.8	0.016	110.5	57.36	57.52
2	Center	0	0	0	6.8	0.016	60	99.71	99.37
3	Factorial	-1	+1	-1	3.2	0.020	30	46.94	46.97
4	Factorial	-1	-1	-1	3.2	0.012	30	40.25	40.28
5	Axial	0	0	-α	6.8	0.016	9.5	65.47	65.38
6	Factorial	+1	+1	+1	10.4	0.020	90	65.26	65.19
7	Factorial	+1	+1	-1	10.4	0.020	30	81.21	81.24
8	Axial	0	-α	0	6.8	0.009	60	66.36	66.39
9	Factorial	-1	-1	+1	3.2	0.012	90	47.06	46.98
10	Center	0	0	0	6.8	0.016	60	99.71	99.37
11	Center	0	0	0	6.8	0.016	60	99.71	99.37
12	Axial	+α	0	0	12.9	0.016	60	36.79	36.82
13	Factorial	+1	-1	+1	10.4	0.012	90	47.29	47.21
14	Axial	-α	0	0	0.75	0.016	60	7.78	7.81
15	Center	0	0	0	6.8	0.016	60	99.71	99.37
16	Center	0	0	0	6.8	0.016	60	99.71	99.37
17	Axial	0	+α	0	6.8	0.022	60	87.1	87.13
18	Center	0	0	0	6.8	0.016	60	99.71	99.37
19	Factorial	+1	-1	-1	10.4	0.012	30	43.74	43.77
20	Factorial	-1	+1	+1	3.2	0.020	90	34.26	34.18

where Y, X_i and X_j are predicted response (removal efficiency), coded values of input factors (i = 1 → 3; j = 1 → 3; i ≠ j) and β₀, β_i, β_{ij} and β_{ijj} are coefficients for the intercept, linear, quadratic and interaction terms, respectively. ε is the random error of the model.

2.5. Isotherm studies

Adsorption studies were conducted in batch mode at different temperatures (305, 310, 315 and 320 K). The solution pH was adjusted with HCl or NaOH solution. A known amount of MPA/HZO (0.016 g) was kept in a series of 50 mL flasks having Pb (II) solution (20 mL) of varying concentrations (9.5–110.5 mg/L) at pH 6.8 and then agitated (150 rpm) in a water bath shaker for 40 min. After filtration the concentration of Pb (II) in the filtrate was measured using AAS. The removal efficiency (%) and sorption capacity (q_e; mg/g) were obtained from Eqs (3) and (4), respectively:

$$\text{Removal efficiency (\%)} = \frac{C_0 - C_e}{C_0} 100 \tag{3}$$

$$q_e = \frac{(C_0 - C_e) V}{M} \tag{4}$$

where q_e (mg/g) is the quantity of Pb(II) adsorbed at equilibrium. C₀ and C_e represent the initial and equilibrium concentrations (mg/L), respectively. V and M are solution volume (L) and mass of the MPA/HZO (g), respectively.

2.6. Kinetic studies

The adsorption kinetic studies were performed by adding 0.016 g MPA/HZO in a series of 50 mL flasks having 20 mL of Pb (II) solutions (60 mg /L, pH 6.8). The resulting mixtures were agitated (150 rpm) at 305, 310, 315 and 320 K in water bath shaker for different time intervals. The flasks were removed from the shaker at the desired time interval and the residual concentration of Pb(II) in solution was obtained by AAS. Finally, the adsorbed amounts of Pb(II) (q_e) at different time interval were calculated and used in the investigation of different kinetic models.

2.7. Nonlinear regression analysis and error functions

In this study, all the kinetic and isotherm model parameters were evaluated by nonlinear regression analysis using the reported method (Hossain et al., 2013; Rahman and Varshney, 2020). Error functions were used to judge the best kinetic and isotherm models to describe the interface interactions and nature of adsorption process. Statistical error functions such as sum of squares of the error (SSE), sum of the absolute error (SAE), chi-square test (χ²) and Spearman’s correlation coefficient (r_s) were evaluated using the following equations.

$$SSE = \sum_{i=1}^N (q_{e,cal} - q_{e,exp})_i^2 \tag{5}$$

$$SAE = \sum_{i=1}^N |q_{e,cal} - q_{e,exp}|_i \tag{6}$$

$$\chi^2 = \sum_{i=1}^N \frac{(q_{e,exp} - q_{e,cal})^2}{q_{e,cal}} \tag{7}$$

$$r_s = 1 - \frac{6 \sum_{i=1}^N (q_{e,exp} - q_{e,cal})^2}{N(N^2 - 1)} \tag{8}$$

The terms q_{e,cal} and q_{e,exp} are the simulated and experimental adsorption capacity (mg/g), respectively. N represents total number of data points.

3. Results and discussion

3.1. Characterization

FTIR spectra of HZO and MPA/HZO are shown in Fig. 1a (I & II). Fig. 1aI displayed a broad absorption band peaking at 3429 cm⁻¹ which defines the O–H stretching vibration of coordinated water. The absorption band appearing at 1629 cm⁻¹ signifies the H–O–H bending mode (Rahman et al., 2015). The absorption peak at 1400 cm⁻¹ indicated the O–H bending vibration of Zr–OH group (Zong et al., 2013). The lattice vibration of Zr–O was confirmed by the absorption bands at 848 cm⁻¹, 676 cm⁻¹ and 469 cm⁻¹. The FTIR spectrum of MPA/HZO (Fig. 1aII) exhibited absorption band between 3600 and 3200 cm⁻¹ centred at 3406 cm⁻¹ is attrib-

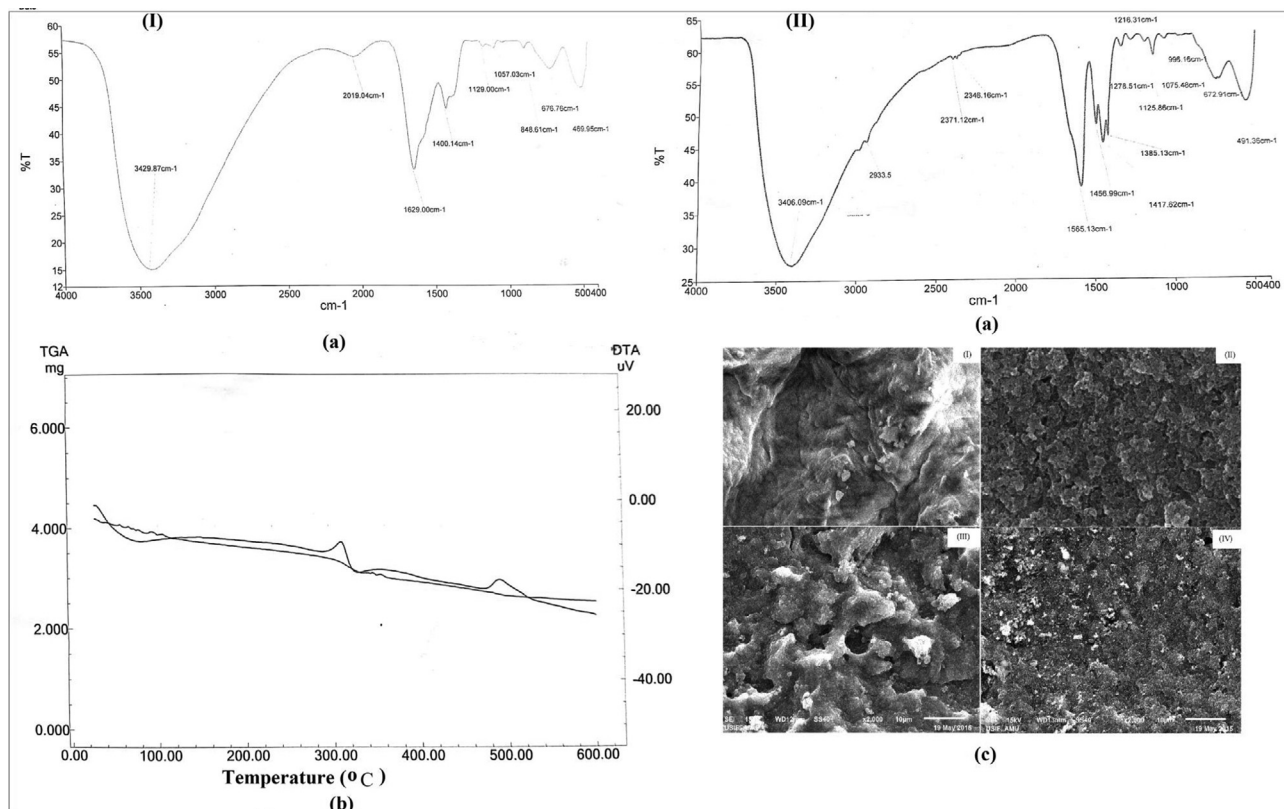


Fig. 1. (a) FTIR spectra, of (I) HZO (II) MPA/HZO (b) TGA-DTA of MPA/HZO and (c) SEM images of (I) HZO, (II) MPA, (III) MPA/HZO and Pb(II) sorbed MPA/HZO.

uted to O–H vibrations. The band appearing at 2933 cm⁻¹ defines the vibration of C–H of CH₃ group. A sharp peak at 1565 cm⁻¹ was designated to COO⁻ stretching vibration (Sakellari et al., 2020). The absorption band at 1075 cm⁻¹ can be assigned to C–S stretching (Scorates, 1980). The bands peaking at 1417 cm⁻¹ and 1278 cm⁻¹ were due to O–H in-plane and C–O–H stretching vibrations, respectively. The thermal stability of MPA/HZO material was examined and thermogravimetric curves are shown in Fig. 1b. The TGA curve shows 15.55% weight loss between 40 °C and 120 °C that can be assigned to the elimination of water molecules. The endothermic peak at 90 °C (DTA curve, Fig. 1b) confirmed the dehydration of MPA/HZO. The second weight loss (17.11%) occurred in the temperature range 100 °C to 340 °C which may be due to the thermal degradation of thiol group of organic moiety and is also confirmed by exothermic peak at 325 °C in DTA curve. The continuous weight loss (12.69%) from 300 °C to 520 °C may be due to breakdown of remaining organic moiety and also confirmed by the presence of an exothermic peak in DTA curve at 490 °C. Fig. 1c (I–IV) shows the SEM images of HZO, MPA, MPA/HZO and Pb(II) sorbed MPA/HZO, respectively. It was apparent that SEM image of HZO (Fig. 1cI) exhibited the irregular surfaces. The surface morphology of MPA (Fig. 1cII) pointed towards rugged surface consisting of particles of different sizes and shapes with voids spaces. The surface morphology was changed when MPA was impregnated on the surface of HZO. The surface of MPA/HZO was slightly changed on Pb(II) adsorption. The presence of Zr, C, S and O in the EDX spectrum (Fig. S1) also confirmed the synthesis of MPA/HZO.

3.2. RSM and statistical analysis

The experiments were conducted following the CCD matrix and the results (Table 1) were fitted to quadratic model to generate the regression equation. The correlation between the predicted response (% Removal) and the selected variables is expressed as:

$$\text{Removal (\%)} = + 99.37 + 8.62 X_1 + 6.17 X_2 - 2.34 X_3 + 7.69 X_1 X_2 - 0.8162X_1X_3 - 4.87X_2X_3 - 27.24X_1^2 - 7.99X_2^2 - 13.41X_3^2 \quad (9)$$

Results of analysis of variance (ANOVA) are presented in Table 2. The larger magnitude of F-values and smaller p-values (<0.05) illustrate the adequacy of model and model terms. In this study, the higher F-value (14916.48) and lower p-value (<0.0001) of quadratic model and the lowest F-value (0.0195) and high p-value (0.9997) of lack of fit confirmed that quadratic model is highly significant with insignificant lack of fit. Moreover, all model terms have p-values < 0.05 and hence, all these terms are significant.

The high values of R² (0.9997), adjusted R² (0.9996) and predicted R² (0.9996) for the quadratic model demonstrated that an excellent relationship existed between the experimental and the predicted responses. The low values of coefficient of variation (C.V = 0.8812%) and standard deviation (0.5829) suggested that degree of precision was satisfactory. The lowest predicted residual error sum of squares (PRESS) value (9.13) indicated that the quadratic model fits each point in the design (Fig. S2). The value of adequacy precision is used to measure signal to noise ratio and if its value is greater than 4, then this adequate signal is capable to navigate the design space. In the present study higher adequacy precision value (222.1264) confirmed that quadratic model was used to direct the design space. The variance inflation factor (VIF) examines the degree of correlation between the coefficients of independent variables (Zhang et al., 2020). The value of VIF equal to 1.00 indicated that all three factors are orthogonal to each other.

3.3. Effects of variables and response surface plots

Regression equation is graphically represented by 3D-response surface plots. From 3D-response surface plots, it can be easily deduced the importance of binary interactions between the

Table 2
Sequential sum of squares, analysis of variance (ANOVA) and goodness of fit.

Source	Sum of square	df	Mean square	F-value	P-value	Remarks
Sequential sum of square						
Mean vs total	87533.65	1	87533.65			
Linear vs Mean	1609.55	3	536.52	0.6449	0.5973	
2FI vs Linear	668.91	3	222.97	0.2293	0.8743	
Quadratic vs 2FI	12638.02	3	4212.67	12396.85	< 0.0001	Suggested
Residual	3.34	6	0.5574			
Total	1.025E + 05	16	5122.66			
Analysis of variance (ANOVA)						
Model	14916.48	9	1657.39	4877.28	<0.0001	Significant
X ₁ -pH	1015.74	1	1015.74	2989.08	<0.0001	
X ₂ -Adsorbent dose	519.25	1	519.25	1528.04	< 0.0001	
X ₃ -Initial Concentration	74.56	1	74.56	219.40	<0.0001	
X ₁ X ₂	473.55	1	473.55	1393.54	<0.0001	
X ₁ X ₃	5.33	1	5.33	15.69	0.0027	
X ₂ X ₃	190.03	1	190.03	559.20	<0.0001	
X ₁ ²	10696.25	1	10696.25	31476.42	< 0.0001	
X ₂ ²	921.03	1	921.03	2710.35	<0.0001	
X ₃ ²	2591.19	1	2591.19	7625.22	<0.0001	
Residual	3.40	10	0.3398			
Lack of Fit	0.0648	5	0.0130	0.0195	0.9997	Not significant
Pure Error	3.33	5	0.6667			
Cor Total	14919.88	19				
Goodness of fit						
Std. Dev.	0.5829		R ²	0.9998		
Mean	66.16		Adjusted R ²	0.9996		
C.V. %	0.8812		Predicted R ²	0.9996		
PRESS	5.29		Adeq Precision	222.1264		
VIF	1.0					

selected process variables on the response. The influence of equilibrating time on the adsorption process is displayed in Fig S3 and found that the equilibrium was achieved at 40 min. Fig. 2a shows the interactive effects of pH and adsorbent mass on the removal efficiency while keeping the initial concentration at the centre level. At any fixed amount of adsorbent the uptake increased with pH and highest removal was observed at pH 6.8. At pH < 5, the adsorbent surface is positively charged due to the presence of SH₂⁺ and Zr-OOH⁺ and hence, electrostatic repulsion between Pb (II) ions and the positively charged adsorbent surface resulted in decrease in removal efficiency. Above pH 7, the uptake of Pb(II) decreases. The maximum removal (99.37%) of Pb(II) was realized with 0.016 g of MPA/HZO at pH 6.8. The interactive effects of pH and initial concentration (Fig. 2b) suggested that at constant adsorbent dose (0.016 g) the sorption efficiency increased with increasing the Pb(II) concentration at any given pH value. The maximum uptake was observed when the initial concentration of Pb(II) was 60 mg/L. The combined effects of adsorbent mass and initial con-

centration on the uptake of Pb(II) (Fig. 2c) revealed that at constant pH (6.8) the Pb(II) removal efficiency was found to increase with increasing both adsorbent mass and initial concentration. At the optimum concentration (60 mg/L) the percentage removal increased from 42.69 to 99.37% when the adsorbent mass was altered from 0.009 to 0.016 g. These results revealed that the highest removal of Pb(II) (99.37%) was brought out when the pH, adsorbent mass and initial concentration were 6.8, 0.016 g and 60 mg/L, respectively.

3.4. Isotherm studies

In order to understand the nature of adsorption, the adsorption data were analyzed by (i) two- parameters isotherm models namely Langmuir, Freundlich, and Temkin and (ii) three- parameters isotherm models such as Redlich-Peterson, and Sips. The non-linear equations of these isotherm models are given in Table 3. The isotherm parameters were computed using nonlinear regression

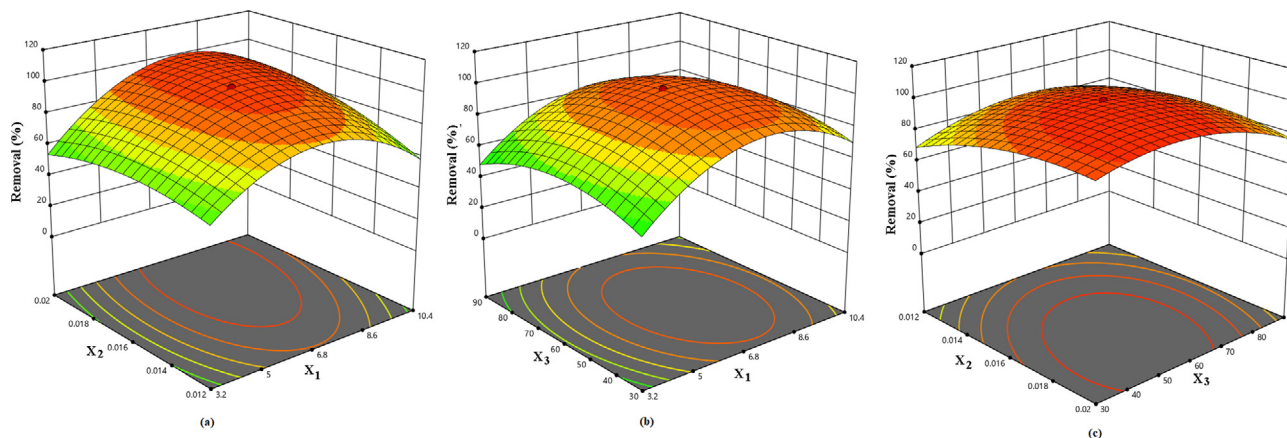


Fig. 2. Response surface plots show the effects of (a) pH and adsorbent dose (b), pH and initial concentration (c) and adsorbent dose and initial concentration on the removal of Pb (II) by MPA/HZO.

approach. The error functions such as SSE, SAE, χ^2 and Spearman's correlation coefficient (r_s) were calculated for each isotherm model.

Two-parameters isotherm models

Fig. 3 represents C_e versus q_e , predicted by nonlinear method, plots for (a) Langmuir, (b) Freundlich and (c) Temkin models at 305, 3010, 315 and 320 K. In case of Langmuir model, the low values of SSE, SAE and χ^2 with high r_s values (0.999) suggested that Langmuir isotherm equation was fitted well to experimental equilibrium data. On the basis of low error values with high values of r_s (0.999), the order of best fit of two-parameters equation was Langmuir > Temkin > Freundlich. The results indicated that the homogeneous surface of MPA/HZO is involved in the uptake of Pb(II). Moreover, a dimensionless constant (R_L) was evaluated from the Langmuir isotherm constant (K_L) using Eq.(10).

$$R_L = \frac{1}{1 + K_L C_0} \tag{10}$$

where C_0 (mg/L) is the initial concentration. The adsorption is favorable when $0 < R_L < 1$. Herein, R_L values were <0.20 at all temperatures and concentrations studied which pointed towards favourable adsorption of Pb(II) onto MPA/HZO. Similar observations were reported for the uptake of Pb(II) onto silica gel functionalized with thiosalicylic acid (Rahman et al., 2021).

Three-parameters isotherm models

The Redlich-Peterson isotherm model (Redlich and Peterson, 1959) is a hybrid form of Langmuir and Freundlich isotherm models and applied for both homogenous and heterogeneous systems. The exponent term of Redlich-Peterson (g) should lie between 0 and 1. If the value of g is closed to unity or equal to unity, then Redlich-Peterson isotherm model behave like Langmuir isotherm

model (Choi and Lee, 2020). The plots of Redlich-Peterson isotherm model at four different temperatures (305, 310, 315 and 320 K) are presented in Fig. 3d. The high values of r_s (>0.99) and low error values (Table 3) confirmed the applicability of this model. Furthermore, the values of exponent terms (g) was very close to unity (0.925–0.987), indicated that the sorption process was most likely occurred on homogeneous surface.

Sips isotherm model (Sips, 1948) is also known as Langmuir–Freundlich isotherm model. At low adsorbate concentration it takes the form of Freundlich model (N'diaye and Kankou, 2020), while at high adsorbate concentration it behaves as Langmuir model., Sips model (Table 3, Fig. 3e) shows low error values with high r_s -values (>0.99) at all studied temperatures. The exponent values were found close to unity (0.913–0.892). Further, it is suggested that Langmuir model was the most suitable to describe the adsorption of Pb (II) onto MPA/HZO. It was judged that adsorption of Pb(II) occurred on homogeneous surface with monolayer coverage most preferably as compared to those on heterogeneous surface with multilayer coverage.

3.5. Adsorption kinetics

To gain an insight into mechanism of the uptake of Pb (II) onto MPA/HZO, pseudo-first order, pseudo-second order, Elovich and intraparticle diffusion models were applied to the experimental kinetic data. The kinetic equations of various models are given in Table 4. The suitability and adequacy of the kinetic model was judged on the basis of high Spearman's correlation coefficient (r_s) and low values of error functions.

3.5.1. Surface based kinetics

The pseudo-second order kinetic model (Fig. 4a) exhibited lower values of error functions with high r_s -values (0.9991–0.9995) as compared to those obtained for the pseudo-first order

Table 3 Nonlinear isotherm equations, isotherm parameters and error values for the adsorption of Pb(II) onto MPA/HZO.

Two-parameters isotherm model		Tem (K)	Parameters				Error function				
Non-linear equation			* q_e (mg/g)	K_F	n	R^2	SSE	SAE	r_s	χ^2	
Freundlich	$q_e = k_F C_e^{1/n}$	307	130.722	62.892	3.827	0.9999	4.805	2.192	0.987	0.037	
		312	137.167	71.289	4.527	0.9999	22.420	4.735	0.971	0.169	
		317	139.047	85.370	5.201	0.9999	17.164	4.143	0.896	0.127	
		322	142.167	98.653	5.984	0.9999	35.236	5.936	0.786	0.258	
Langmuir	$q_e = \frac{q_m K_L C_e}{1 + K_L C_e}$	307	128.498	2.279		0.9999	1.000×10^{-3}	0.032	0.999	7.962×10^{-6}	
		312	132.412	4.304		0.9999	4.000×10^{-4}	0.020	0.999	3.024×10^{-6}	
		317	134.796	5.621		0.9999	0.012	0.101	0.999	7.562×10^{-5}	
		322	136.101	6.987		0.9999	0.017	0.130	0.999	1.241×10^{-4}	
Temkin	$q_e = \beta \ln A_T C_e$	307	127.925	27.524	A_T	0.9998	2.298	1.516	0.986	0.017	
		312	130.684	24.362	36.987	0.9998	0.312	0.559	0.997	0.002	
		317	131.834	20.379	50.347	0.9999	3.470	1.863	0.988	0.025	
		322	132.729	15.358	70.628	0.9994	0.253	0.502	0.997	0.002	
Three-parameters isotherm											
Redlich-Peterson	$q_e = \frac{K_R C_e}{1 + a_R C_e^g}$		K_R	a_R	g						
		307	128.142	8.341	127.397	0.987	0.9998	0.151	0.388	0.999	8.017×10^{-4}
		312	132.106	11.546	131.587	0.925	0.9999	0.106	0.327	0.999	6.132×10^{-4}
		317	134.012	15.375	133.985	0.957	0.9999	0.786	0.887	0.995	0.005
Sips	$q_e = \frac{K_S C_e^g}{1 + a_S C_e^g}$		α	K_S	a_S						
		307	129.014	0.532	127.651	0.892	0.9998	0.234	0.481	0.998	0.002
		312	132.875	0.501	132.089	0.902	0.9997	0.196	0.443	0.999	0.001
		317	134.999	0.476	134.582	0.909	0.9999	0.010	0.101	0.999	7.562×10^{-5}
322	137.296	0.392	136.983	0.913	0.9998	1.132	1.064	0.993	0.0083		

where q_e : experimental adsorption capacity(mg/g), q_m : calculated adsorption capacity (mg/g), C_e : equilibrium concentration (mg/L), K_L : Langmuir isotherm constant (L/mg), k_F & $\frac{1}{n}$ are Freundlich isotherm constants, A_T & β are Temkin isotherm constants related to equilibrium binding constant and adsorption heat, respectively, a_R (L/mg) and K_R (L/g): the Redlich-Peterson constant, g is the exponent; K_S (L/g) and B (L/g): Sips isotherm constant and α is exponent term, * $q_{e,exp}$ at 307, 312, 317 and 322 K are 128.530, 132.432, 134.897 and 136.231, respectively. Experimental conditions are adsorbent dose = 0.016 g /20 mL; pH = 6.5; contact time 40 min.

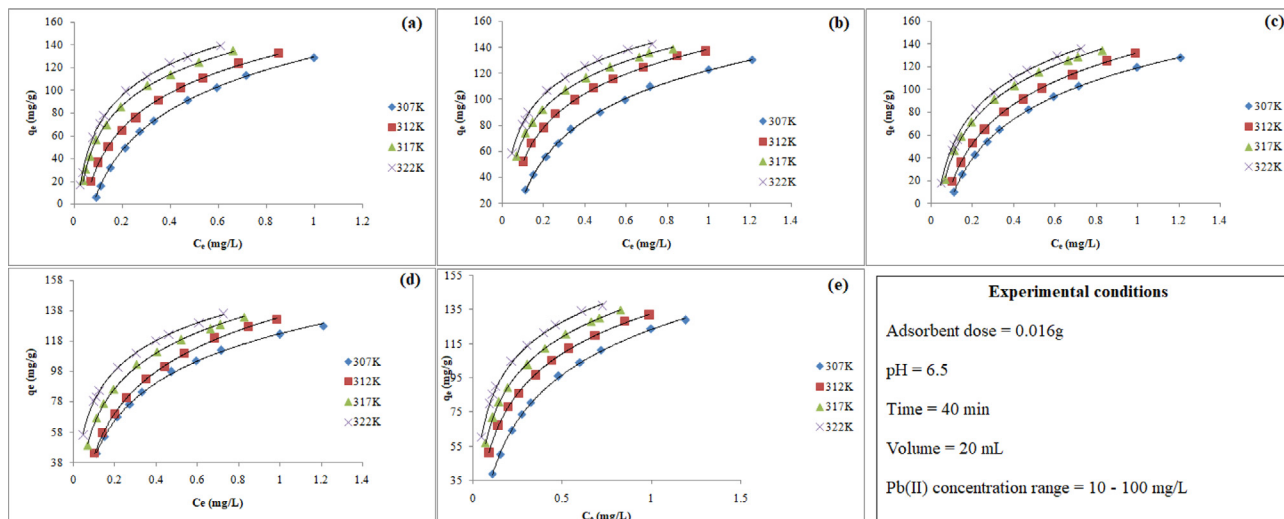


Fig. 3. Nonlinear isotherm plots of (a) Langmuir, (b) Freundlich (c) Temkin, (d) Redlich-Peterson, and (e) Sips for the adsorption of Pb (II) onto MPA/HZO.

Table 4

Non-linear kinetic equations, parameters and statistical error values for the adsorption of Pb(II) onto MPA/HZO.

Kinetic models*	Non-linear equation	Temp (K)	Parameters			Error Values				
			**qe (mg/g)	k ₁	R ²	SSE	SAE	r _s	χ ²	
PFO	$q_t = q_e(1 - e^{-k_1 t})$	307	25.623	0.059	0.9991	1.993	1.412	0.762	0.073	
		312	28.348	0.072	0.9994	2.992	1.73	0.714	0.992	
		317	32.371	0.098	0.9990	1.827	1.352	0.797	0.054	
		322	35.067	0.121	0.9991	1.638	1.280	0.849	0.049	
PSO	$q_t = \frac{k_2 q_e^2 t}{1 + k_2 q_e t}$	307	27.001	k ₂ 0.002	0.9999	0.001	0.034	0.999	4.274 × 10 ⁻⁵	
		312	30.040	0.004	0.9999	0.001	0.038	0.999	4.800 × 10 ⁻⁵	
		317	33.702	0.008	0.9999	4.410 × 10 ⁻⁴	0.021	0.999	1.307 × 10 ⁻⁵	
		322	36.339	0.012	0.9999	3.240 × 10 ⁻⁵	0.018	0.999	8.901 × 10 ⁻⁶	
Elovich	$q_t = \frac{1}{\beta} \ln(1 + \alpha \beta t)$	307	27.274	α 139.324	β 0.268	0.9999	0.057	0.239	0.996	0.002
		312	30.330	248.960	0.259	0.9999	0.063	0.252	0.993	0.002
		317	33.914	298.642	0.234	0.9999	0.036	0.191	0.997	0.001
		322	36.435	387.963	0.221	0.9999	0.007	0.088	0.999	2.130 × 10 ⁻⁴

where q_e and q_t are adsorption capacities of adsorption (mg/g) at equilibrium and time t, respectively. K₁; rate constant (min⁻¹) of the model (PFO), k₂; PSO rate constant (g/mg/min), α; initial adsorption rate (mg/g min) and β; desorption constant (mg/g) and activation energy for chemisorption.

*PSO and PFO are the abbreviation of pseudo-first order and pseudo-second order kinetic models, respectively. **q_{e, exp} at 305, 310, 315 and 320 K are 27.035, 30.078, 33.723 and 36.347, respectively. Experimental conditions are C₀ = 30 mg/L; adsorbent dose = 0.016 g /20 mL; pH = 6.8.

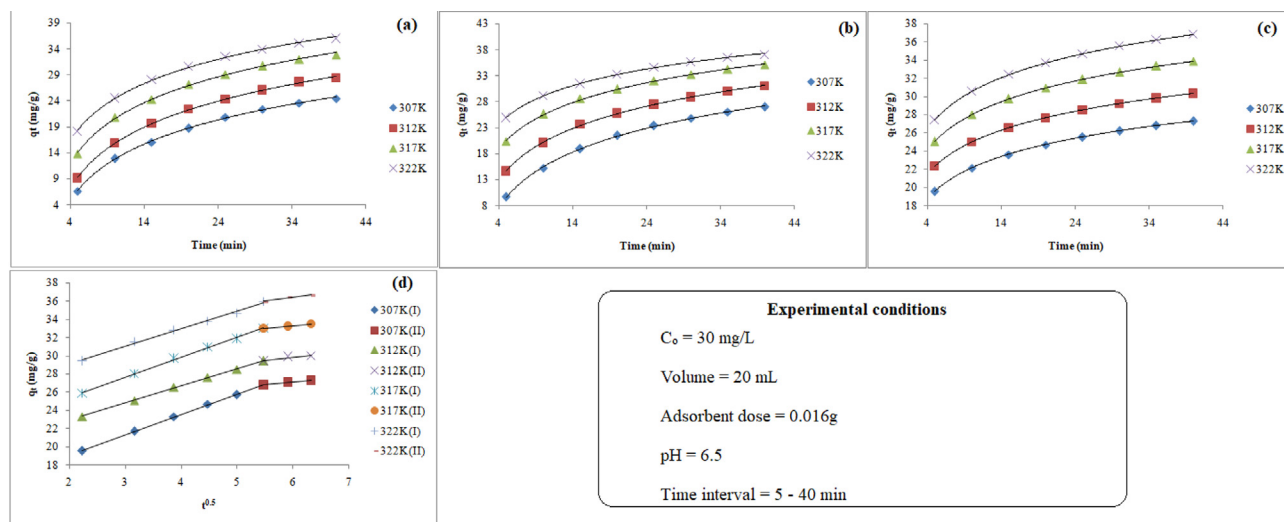


Fig. 4. Nonlinear kinetic plots of (a) pseudo-first order, (b) pseudo second order (c) Elovich models and (d) plots of Weber-Morris intraparticle diffusion model for the adsorption of Pb(II) onto MPA/HZO.

Table 5
Weber-Morris intraparticle diffusion model's equation and parameters for the adsorption of Pb(II) onto MPA/HZO.

Diffusion model	Equation	Plot	Temperature (K)	Parameters			
				Linear portion	K_{id}	C_{id}	R^2
Intraparticle diffusion	$q_t = K_{id} t^{0.5} + C_{id}$	q_t vs $t^{0.5}$	307	I	2.234	14.610	0.999
				II	0.559	23.741	0.997
			312	I	2.194	19.153	0.997
				II	0.609	25.701	0.998
			317	I	1.907	21.042	0.999
				II	0.690	29.364	0.995
			322	I	1.883	25.324	0.998
				II	0.822	29.698	0.997

where k_{id} and C_{id} are intraparticle diffusion constant and the mass transfer across the boundary layer constant, respectively.

kinetic model (Fig. 4b) at all studied temperatures. Furthermore, the value of rate constants (both pseudo first and pseudo second order kinetic models) increases with increasing temperatures, suggested that the mobility of Pb(II) was- increased with rise in temperature. Therefore, the results recommended that the adsorption of Pb(II) onto MPA/HZO might be chemisorption. To confirm the chemisorption behaviour of the adsorption process, the experimental data were further examined by Elovich model (Fig. 4c). As can be seen in the Table 4, Elovich model exhibits low error and high r_s -values (0.9979–0.9991) at all studied temperatures and hence, illustrated that chemisorption also takes place in addition to ion exchange. The value of α increases with increasing the temperature whereas a slight change was observed in case of β , suggested that the sorption rate of Pb(II) onto MPA/HZO was increased with increasing the temperature but the desorption process was negligibly affected.

3.5.2. Diffusion based kinetics

The diffusion mechanism of Pb(II) into MPA/HZO was investigated by using Weber-Morris intraparticle diffusion model. The plots of q_t vs $t^{0.5}$ (Fig. 4e) showed two distinct linear segments (I and II) suggesting that two stages were involved during the sorption process. The first linear portion (stage I) shows that the adsorption rate was rapid upto 25 min which was due to external surface adsorption (boundary-layer diffusion) from aqueous phase to surface of the adsorbent. Second linear portion (stage II) shows the slow adsorption rate which pointed towards intraparticle diffusion. The values of intraparticle diffusion constant (k_{id}) and the boundary layer thickness (C_{id}) were calculated from the slope and intercept of the intraparticle diffusion plots. It is evident from the Table 5 that the value of K_{id} decreases in the first stage whereas increases in second stage with increasing temperature. The contribution of boundary layer (C_{id}) increased during the mass transfer and decreased during the intraparticle diffusion with increasing the temperature. Therefore, it is concluded that during the mass transfer the sorption of Pb(II) can be controlled by two mechanisms: external surface adsorption (boundary-layer diffusion); and intraparticle diffusion.

4. Conclusions

MPA/HZO was synthesized and used as sorbent for Pb(II) removal. Under the optimum conditions (pH: 6.8; adsorbent dose: 0.016 g; initial Pb(II) concentration: 60 mg/L), 99.37% Pb(II) was removed from the aqueous solution. The experimental equilibrium data were analyzed by two- and three- parameters isotherm models using nonlinear regression analysis.

High values of Spearman's correlation coefficient (r_s) and low values of various statistical error functions suggested that Langmuir isotherm was the best fitted model followed by Temkin and Freundlich isotherm models in case of two-parameters models. In case of three-parameters model, fitting of the experimental data

followed the order Redlich-Peterson > Sips. The kinetic data followed the pseudo second order model. Therefore, it is concluded that MPA/HZO could be a potential and efficient adsorbent in the remediation of Pb(II) from contaminated water.

Declaration of Competing Interest

The authors declare that they have no known competing financial interests or personal relationships that could have appeared to influence the work reported in this paper.

Acknowledgments

The authors extend their appreciation to the Deputyship for Research & Innovation, "Ministry of Education" in Saudi Arabia for funding this research work through the project number IFKSURG-1435-010.

Appendix A. Supplementary data

Supplementary data to this article can be found online at <https://doi.org/10.1016/j.jksus.2020.101280>.

References

- Azamfire, B., Bulgariu, D., Bulgariu, L., 2020. Efficient removal of toxic metal ions (Pb (II) and Hg(II) ions in single component systems by adsorption on Romanian clay material. *Rev. Chim.* 71, 37–47. <https://doi.org/10.37358/RC.20.7.8223>.
- Azmi, S.N.H., Al-Balushi, M., Al-Siyabi, F., Al-Hinai, N., Khurshid, S., 2020. Adsorptive removal of Pb(II) ions from groundwater samples in Oman using carbonized Phoenix dactylifera seed (Date stone). *J. King Saud University – Sci.* 32 (7), 2931–2938. <https://doi.org/10.1016/j.jksus.2020.07.015>.
- Boni, M.R., Chiavola, A., Marzeddu, S., 2020. Remediation of lead-contaminated water by virgin coniferous wood biochar adsorbent: batch and column application. *Water Air Soil Pollut.* 231, 171–186. <https://doi.org/10.1007/s11270-020-04496-z>.
- Bora, A.J., Dutta, R.K., 2019. Removal of metals (Pb, Cd, Cu, Cr, Ni, and Co) from drinking water by oxidation-coagulation-adsorption at optimized pH. *J. Water Process Eng.* 31, 100839. <https://doi.org/10.1016/j.jwpe.2019.100839>.
- Boudrahem, F., Aissani-Benissad, F., Soualah, A., 2011. Adsorption of Lead(II) from Aqueous Solution by Using Leaves of Date Trees As an Adsorbent. *J. Chem. Eng. Data* 56 (5), 1804–1812. <https://doi.org/10.1021/je100770j>.
- Choi, J.-H., Lee, C.-H., 2020. Adsorption kinetic and isotherm characteristics of Mn ions with zeolitic materials synthesized from industrial solid waste. *J. Environ. Sci. Int.* 29, 827–835.
- Gupta, V.K., Singh, P., Rahman, N., 2005. Synthesis, characterization, and analytical application of zirconium(IV) selenoiodate, a new cation exchanger. *Anal Bioanal Chem* 381 (2), 471–476. <https://doi.org/10.1007/s00216-004-2949-7>.
- Gupta, V.K., Singh, P., Rahman, N., 2004. Adsorption behavior of Hg(II), Pb(II), and Cd (II) from aqueous solution on Duolite C-433: a synthetic resin. *J. Colloid Interface Sci.* 275 (2), 398–402. <https://doi.org/10.1016/j.jcis.2004.02.046>.
- Halli, P., Agarwal, V., Partinen, J., Lundström, M., 2020. Recovery of Pb and Zn from a citrate leach liquor of a roasted EAF dust using precipitation and solvent extraction. *Sep. Purif. Technol.* 236, 116264. <https://doi.org/10.1016/j.seppur.2019.116264>.
- Hossain, M.A., Ngo, H.H., Guo, W., 2013. Introductory of Microsoft Excel SOLVER function spread sheet method for isotherm and kinetics modelling of matelsbiosorption in wastewater. *J. Water Sustainability* 3, 223–227.

- Jiang, C., Wang, X., Hou, B., Hao, C., Li, X., Wu, J., 2020. Construction of a Lignosulfonate–Lysine Hydrogel for the Adsorption of Heavy Metal Ions. *J. Agric. Food Chem.* 68 (10), 3050–3060. <https://doi.org/10.1021/acs.jafc.9b07540.s001>.
- Kumar, A., Kumar, A., Cabral-Ointo, M.M.S., et al., mar et al., Lead toxicity: health hazards, influence on food chain, and sustainable remediation approaches. *Int. J. Environ. Res. Public Health* 17, 2179. <https://doi.org/10.3390/ijerph17072179>.
- Lutfullah, ., Rashid, M., Rahman, N., 2012a. Synthesis, Characterization and Sorption Characteristics of a Fibrous Organic–Inorganic Composite Material. *Adv. Sci. Lett.* 17 (1), 136–142. <https://doi.org/10.1166/asl.2012.3691>.
- Lutfullah, ., Rashid, M., Rahman, N., 2012b. Zirconium(IV) Phosphosulphosalicylate as an Important Lead(II) Selective Ion-Exchange Material: Synthesis, Characterization and Adsorption Study. *Adv. Sci. Lett.* 17 (1), 184–190. <https://doi.org/10.1166/asl.2012.3683>.
- Moja, T.N., Bunekar, N., Mishra, S.B., Tsai, T.-Y., Hwang, S.S., Mishra, A.K., 2020. Melt processing of polypropylenegrafted-maleic anhydride/chitosan polymer blend functionalized with montmorillonite for the removal of lead ions from aqueous solutions. *Sci. Rep.* 10, 217–231. <https://doi.org/10.1038/s41598-019-57079-2>.
- Ndiaye, A.D., Kankou, M.S.A., 2020. Modeling of adsorption isotherms of pharmaceutical products onto various adsorbents: A Short Review. *J. Mater. Environ. Sci.* 11, 1264–1276.
- Nordin, N.A., Rahman, N.A., Abdullah, A.H., 2020. Effective removal of Pb(II) ions by electrospun PAN/sago lignin-based activated carbon nanofibers. *Molecules* 25, 3081. <https://doi.org/10.3390/molecules25133081>.
- Rahman, N., Haseen, U., 2014. Equilibrium Modeling, Kinetic, and Thermodynamic Studies on Adsorption of Pb(II) by a Hybrid Inorganic–Organic Material: Polyacrylamide Zirconium(IV) Iodate. *Ind. Eng. Chem. Res.* 53, 8198–8207.
- Rahman, N., Haseen, U., Khan, M.F., 2015. Cyclic tetra[(indolyl)-tetra methyl]-diethane-1,2-diamine (CTet) impregnated hydrous zirconium oxide as a novel hybrid material for enhanced removal of fluoride from water samples. *RSC Adv.* 5, 39062–39074.
- Rahman, N., Haseen, U., Rashid, M., 2017. Synthesis and characterization of polyacrylamide zirconium(IV) iodate ion exchanger. Its application of selective removal of lead (II) from wastewater. *Arabian J. Chem.* 10, S1765–S1773. <https://doi.org/10.1016/j.arabjc.2013.06.029>.
- Rahman, N., Nasir, M., 2018. Application of Box–Behnken design and desirability function in the optimization of Cd(II) removal from aqueous solution using poly(o-phenylenediamine)/hydrous zirconium oxide composite: equilibrium modeling, kinetic and thermodynamic studies. *Environ Sci Pollut Res* 25, 26114–26134.
- Rahman, N., Nasir, M., 2019. N-((2-((2-Aminoethyl)amino)ethyl)amino)methyl)-4-sulfamoylbenzamide Impregnated Hydrous Zirconium Oxide as a Novel Adsorbent for Removal of Ni(II) from Aqueous Solutions: Optimization of Variables Using Central Composite Design. *ACS Omega* 4, 2823–2832.
- Rahman, N., Khan, M.F., Nasir, M., 2020. Experimental design approach for optimization of Pb(II) removal from aqueous solution using poly-o-toluidine/stannic(IV) triethanolamine as adsorbent. *Environ. Technol. Innovation* 17, 100634.
- Rahman, N., Nasir, M., Varshney, P., Al-Enizi, A.M., Ubaidullah, M., Shaikh, S.F., Al-Adrabalnabi, M.A., 2021. Efficient removal of Pb(II) from water using silica gel functionalized with thiosalicylic acid: Response surface methodology for optimization. *J. King Saud Univ. Sci.* 33, 101232.
- Rahman, N., Nasir, M., 2020a. Facile synthesis of thiosalicylic acid functionalized silica gel for effective removal of Cr(III): Equilibrium modeling, kinetic and thermodynamic studies. *Environ. Nanotechnol. Monit. Manage.* 14, 100353. <https://doi.org/10.1016/j.enmm.2020.100353>.
- Rahman, N., Nasir, M., 2020b. Effective removal of acetaminophen from aqueous solution using Ca (II)-doped chitosan/ β -cyclodextrin composite. *J. Mol. Liq.* 301, 112454. <https://doi.org/10.1016/j.molliq.2020.112454>.
- Rahman, N., Varshney, P., 2020. Assessment of ampicillin removal efficiency from aqueous solution by polydopamine/zirconium(IV) iodate: optimization by response surface methodology. *RSC Adv.* 10, 20322–20337. <https://doi.org/10.1039/d0ra02061c>.
- Redlich, O., Peterson, D.L., 1959. A Useful Adsorption Isotherm. *J. Phys. Chem.* 63 (6), 1024. <https://doi.org/10.1021/j150576a611>.
- Sips, R., 1948. On the structure of a catalyst surface. *J. Chem. Phys.* 16, 490–495.
- Sakellari, G.I., Hondow, N., Gardinar, P.H.E., 2020. Factors influencing the surface functionalization of citrate stabilized gold nanoparticles with cysteamine, 3-mercaptopropionic acid or L-selenocystine for sensor applications. *Chemosensors* 8, 80. <https://doi.org/10.3390/chemosensors8030080>.
- Scorates, G., 1980. Infrared characteristic group frequencies. *John Wiley & Sons*, New York, p. 112.
- Thaci, B.S., Gashi, S.T., 2019. Reverse osmosis removal of heavy metals from wastewater effluents using biowaste materials. *Pol. J. Environ. Stud.* 28, 337–341. <https://doi.org/10.15244/pjoes/81268>.
- World Health Organization, 2017. Guidelines for drinking-water quality. Fourth edition incorporating the first addendum, Geneva.
- Zhang, Q., Hou, Q., Huang, G., Fan, Q.i., 2020. Removal of heavy metals in aquatic environment by graphene oxide composites: a review. *Environ Sci Pollut Res* 27, 190–209. <https://doi.org/10.1007/s11356-019-06683-w>.
- Zong, E., Wei, D., Wan, H., Zheng, S., Xu, Z., Zhu, D., 2013. Adsorptive removal of phosphate ions from aqueous solution using zirconia-functionalized graphite oxide. *Chem. Eng. J.* 221, 193–203. <https://doi.org/10.1016/j.cej.2013.01.088>.